

Adsorption and Decomposition of Dimethyl Methylphosphonate on Size-Selected Zirconium Oxide Trimer Clusters

Michael A. Denchy, Linjie Wang, Nicolas Blando, Lucas Hansen, Benjamin R. Bilik, Xin Tang, Zachary Hicks, Gerd Gantefoer, and Kit H. Bowen*

Cite This: *J. Phys. Chem. C* 2021, 125, 23688–23698

Read Online

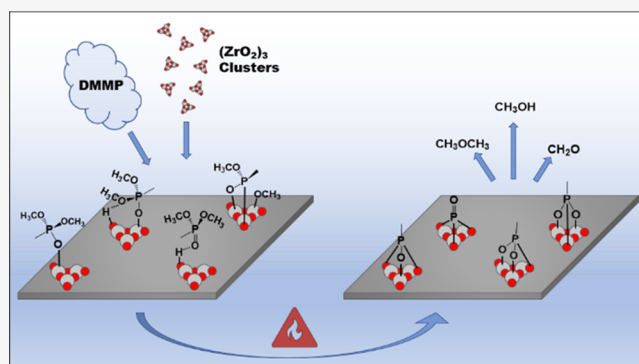
ACCESS |

Metrics & More

Article Recommendations

Supporting Information

ABSTRACT: In recent years, zirconium hydroxide powder and zirconium-based metal organic frameworks have found promising applications as chemical warfare agent (CWA) decomposition materials. While bulk zirconium oxide (ZrO_2) has proven to be relatively inactive for such purposes, well-controlled fundamental studies investigating the potential CWA decomposition propensity of subnanoscale zirconium oxide, in which undercoordinated metal centers abound, are still severely lacking. Herein, the adsorption and decomposition of the nerve agent simulant dimethyl methylphosphonate (DMMP) on size-selected zirconium oxide trimer, that is, $(\text{ZrO}_2)_3$ clusters supported on highly oriented pyrolytic graphite (HOPG), have been investigated via the combination of X-ray photoelectron spectroscopy (XPS) and temperature-programmed desorption/reaction (TPD/R). XPS measurements acquired for the DMMP-adsorbed, HOPG-supported clusters at a preparation temperature of 298 K, and also after annealing to several successively higher temperatures of 473, 573, and 673 K, elucidated the uptake of DMMP to the $(\text{ZrO}_2)_3$ clusters, with one DMMP molecule adsorbed per cluster and virtually no thermal molecular desorption observed up to 673 K. These measurements also showed dissociative adsorption of DMMP at room temperature on some clusters, likely via scission of a P–OCH₃ bond in DMMP, with further decomposition accompanying an increase in temperature above 473 K. TPD/R experiments showed the evolution of methanol as a major reaction product via two distinct pathways, with desorption peaks centered around 410 and 575 K. Evolution of dimethyl ether and formaldehyde as minor reaction products was also observed with desorption peaks centered around 560 and 620 K, respectively. A second TPD/R cycle following cluster-induced DMMP decomposition resulted in no detected decomposition chemistry, showing DMMP decomposition on the $(\text{ZrO}_2)_3$ clusters to be stoichiometric and non-catalytic, whereby the remaining P-containing species poisoned the clusters.



INTRODUCTION

Chemical warfare agents (CWAs) are an ever-present threat across the modern geopolitical landscape. Organophosphorus nerve agents, the most lethal class of CWAs, are among the most toxic chemicals ever synthesized by humans¹ and have reared their ugly head in recent military conflicts and assassinations. Personal protection from CWAs and sensors for reliably detecting CWAs after having been deployed are two important applications that stand to benefit from improved materials.² Their development requires a fundamental chemical understanding of the interaction between CWAs and any potential candidate materials, both in solution³ and heterogeneous gas–surface interface environments.⁴ However, due to the high lethality of nerve agents, civilian research laboratories have been relegated to the use of less toxic simulants, which mimic some properties of live agents, to minimize the risk to researchers and guard against the proliferation of CWAs. A commonly employed nerve agent simulant is dimethyl methylphosphonate (DMMP), especially

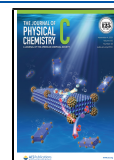
in surface adsorption studies. DMMP has been found to simulate the adsorption behavior of sarin, the most toxic of the G-agent family of nerve agents, especially well. The efficacy of DMMP as an adsorption simulant arises from the relation of its chemical structure to that of sarin, a comparison of which is shown in Figure 1.

While activated carbon was the first filtration material implemented during the First World War to defend against CWAs, eventually transition metal oxide impregnates were included, these imparting increased reactive sorption capability to decompose adsorbed agents.⁵ Today, modern CWA filtration materials are comprised of an ASZM-TEDA

Received: July 7, 2021

Revised: October 13, 2021

Published: October 26, 2021



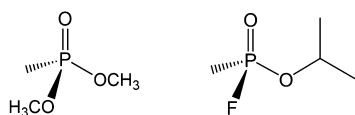


Figure 1. Chemical structures of DMMP (left) and sarin (right).

formulation, in which copper, molybdenum, zinc, and trace amounts of silver metal oxide particles are impregnated into activated carbon filters along with triethylene diamine.⁶ In general, transition metal oxides are a promising class of materials for adsorbing and decomposing CWAs due to their acid/base and redox properties; a robust literature investigating such species has accumulated over the last few decades. Some of the earliest studies that appear in the literature focus on the adsorption and decomposition of DMMP by several transition metal single crystal surfaces, including Rh(100), Pt(111), Mo(110), Ni(111), and Pd(111).^{7–10} In subsequent years, similar studies of DMMP adsorption and decomposition on a range of bulk transition metal oxide species followed, including Al₂O₃,^{11,12} Cu₂O,¹³ CuO,¹⁴ Fe₂O₃,¹⁵ FeO,¹⁶ MgO,¹⁷ MnO,¹⁸ MoO₃,^{19,20} TiO₂,^{21–24} and WO₃.²⁵ Studies of DMMP with several nanosized transition metal oxide materials have also been reported, including MnO₂,^{26,27} Y₂O₃,²⁸ and TiO₂ and ZnO,²⁹ as well as supported metal cluster systems, for example, Cu, Ni, Pt, Au, and Au–Pt clusters supported on TiO₂(110).^{30–32} In addition, we have published work involving mass-selected (MoO₃)₃ and (WO₃)₃ clusters deposited onto a DMMP-laden highly oriented pyrolytic graphite (HOPG) substrate.^{33,34}

One particular transition metal species that has garnered significant attention in recent years is zirconium(IV), especially in the form of zirconium hydroxide, that is, Zr(OH)₄. Bulk Zr(OH)₄ has been found to serve as an effective sorbent for a variety of toxic chemicals including SO₂, CNCl, Cl₂, COCl₂, and HCl,^{35–37} and has also been found to very effectively adsorb and hydrolyze nerve agents VX and soman, as well as the vesicant, sulfur mustard.³⁸ Promising results have also been demonstrated for functional composite materials incorporating Zr(OH)₄ and graphite oxide for adsorbing and decomposing several toxic chemicals including H₂S, SO₂, and sulfur mustard simulant gas, chloroethyl ethyl sulfide.^{39,40} More recently, Zr(OH)₄ has even been successfully incorporated into a nanofibrous mat material that effectively adsorbs and hydrolyzes the reactive nerve agent simulant, diisopropyl fluorophosphate.⁴¹ Further fundamental studies of nanosized Zr(OH)₄ in the form of both nanoparticles⁴² and supported thin films,^{43,44} confirmed the necessity of surface hydroxyls and surface defect sites for the adsorption and decomposition chemistry observed for Zr(OH)₄ materials. Moreover, these studies demonstrated that bulk crystalline samples of the parent material of Zr(OH)₄, that is, zirconium(IV) oxide (ZrO₂), is essentially unreactive toward DMMP decomposition.

While ZrO₂ has had wide success as a catalyst,⁴⁵ largely due to its Lewis acidic properties,⁴⁶ its low activity for DMMP decomposition is likely due to a lack of both coordinatively unsaturated Zr sites and reactive hydroxyl species on its bulk crystal surfaces. Nevertheless, it has become clear over the last few decades that small, nanosized samples of seemingly unreactive species can exhibit widely divergent properties from their larger bulk counterparts.^{47,48} Indeed, the work by Gordon several years ago had shown evidence of exactly this

for small ZrO₂ nanoparticles in their facile adsorption and decomposition of DMMP at room temperature.⁴⁹ Subsequently, an entire family of metal organic framework (MOF) materials exhibiting an exciting degree of hydrolytic decomposition activity toward a host of CWAs and simulants has emerged, in which a partially hydroxylated zirconium(IV) oxide hexamer cluster serves as the active nodal sites of the MOFs.^{50–64} Hence, it is apparent that studies investigating the reactivity of small zirconium oxide clusters toward CWA simulants, such as DMMP, are of great importance in advancing the understanding of CWA decomposition chemistry and the development of future protective materials.

In the present work, the adsorption and decomposition of DMMP by size-selected zirconium(IV) oxide trimer clusters, that is, (ZrO₂)₃, soft-landed onto a HOPG substrate, were investigated. HOPG was chosen as a substrate in these experiments to mimic the carbonaceous material that typically serves as the metal oxide particle support in CWA filtration materials and due to its relatively weak cluster–support interactions. The activity of the HOPG-supported clusters was investigated via the complementary application of X-ray photoelectron spectroscopy (XPS) and temperature-programmed desorption/reaction (TPD/R) experiments. The XPS measurements, acquired after heating to several critical temperatures, served to elucidate the uptake of DMMP by the clusters over a range of temperatures and interrogate the chemical bonding environment of DMMP to the clusters, while the TPD/R experiments served to identify the volatile reaction products evolved from the surface resulting from DMMP decomposition on the clusters as a function of temperature. XPS measurements established strong evidence for substantial DMMP decomposition at room temperature upon adsorption to the clusters, with additional decomposition upon treatment at higher temperatures above 473 K. The TPD/R experiment of the cluster-bound DMMP showed the evolution of volatile decomposition products methanol, dimethyl ether, and formaldehyde. While methanol evolution dominated below 473 K, alternate reaction pathways to dimethyl ether and formaldehyde were accessed at higher temperatures, a phenomenon which has not been reported for DMMP decomposition on other Zr-containing materials to date. Together, these two complementary techniques provide fundamental insights into the interaction of DMMP with (ZrO₂)₃ clusters and the associated decomposition chemistry.

EXPERIMENTAL METHODS

Cluster Synthesis and Deposition. The details of the apparatus used in this work have been described elsewhere.⁶⁵ Zirconium(IV) oxide trimer cluster anions, that is, (ZrO₂)₃[−], were synthesized via reactive magnetron sputtering of a zirconium metal target (Kurt J. Lesker, Grade 702) using a gas mixture of argon (Airgas, 99.999%) and helium (Airgas 99.999%), seeded with oxygen (Airgas 99.994%) via a precision dosing valve (INFICON VDH016-x) having a backing pressure of 15 psi. Ionized argon gas served to sputter the zirconium metal target cathode, which was situated in the magnetic field environment of a cylindrical permanent magnet and electrically biased by as much as −500 V to generate a discharge plasma, while helium served the role of a carrier gas for inducing clustering within the source thermalization region. The synthesized cluster anions were transported via a system of electrostatic ion optics and mass-selected via a magnetic sector mass spectrometer (25° sector, $m/\Delta m = 20$). Following

mass-selection, the cluster anions were focused via a subsequent series of ion optics and soft-landed (<1 eV/atom) onto a grounded HOPG substrate (Bucker, ZYB grade, 12×12 mm², 2 mm thickness) situated in an ultrahigh vacuum (UHV) environment with a base pressure of 1×10^{-9} Torr. Prior to deposition, the HOPG substrate had been freshly cleaved in atmosphere and annealed in vacuo ($T = 773$ K, $\Delta t = 30$ min). Upon deposition, the cluster anions lost their charge to the electrically conductive HOPG surface and became neutral clusters. The resulting cluster discharge current was monitored via a picoammeter and integrated over time to give the total number of clusters deposited, assuming one unit of elementary electric charge per cluster.

For XPS experiments, the HOPG substrate was secured to a tantalum mounting plate via tungsten wires and inserted into a versatile sample holder that allowed for removal of prepared samples and transfer, in vacuo, to an adjacent XPS analysis chamber via a linear manipulator. For TPD/R experiments, the HOPG substrate was mounted on the end of a rotatable three-axis sample manipulator using a sample holder assembly comprised of tantalum foil clips wrapped around two copper leads protruding from the ceramic feedthroughs of a 1.33" diameter power feed/temperature measurement flange (Kurt J. Lesker, TFT1KY2C302). Samples mounted via the TPD/R assembly could be cooled via an internal liquid nitrogen (LN₂) reservoir (to approximately 100 K) in thermal contact with the sample holder assembly. This assembly served to securely hold the HOPG substrate, while simultaneously offering optimal thermal and electrical conductivity for resistive heating (to 773 K) and minimal total surface area of the assembly components, reducing background noise arising from species desorbed from the sample holder assembly during TPD/R experiments.

X-ray Photoelectron Spectroscopy. Samples were prepared by depositing (soft-landing) mass-selected (ZrO₂)₃⁻ cluster anions onto HOPG (6.6×10^{13} clusters, 0.46 clusters/nm²) maintained at room temperature (298 K), while simultaneously exposing the surface to a constant system dose of DMMP ($P_{\text{DMMP}} = 5 \times 10^{-7}$ Torr) via a precision variable leak valve (Varian, 951-5106). This dosing procedure was chosen to maximize the extent of interaction between the clusters and DMMP, as the sample holder used for preparing XPS samples lacked LN₂-cooling capabilities. Prior to dosing, the prepared DMMP sample (Sigma-Aldrich, >97%) was degassed via several freeze-pump-thaw cycles. Following cluster deposition, the prepared samples were transferred in vacuo to a secondary manipulator in an adjacent chamber equipped with XPS instrumentation. Samples transferred to the secondary manipulator were heated via electron bombardment heating using the thermionic emission of a resistively heated tungsten filament positioned directly behind the HOPG substrate mounting plate. The sample temperature was measured via a K-type thermocouple connected to the sample holder on the manipulator. The XPS measurements were taken using non-monochromatic Mg K α X-rays (1253.6 eV) of a Mg/Al dual anode X-ray source (PerkinElmer PHI 04-548) for generating core electron photoemission in the sample, and a hemispherical electron energy analyzer (PerkinElmer PHI 5100 10-360) for analyzing the photoemitted electrons via their kinetic energies.

All XPS spectra were calibrated by graphitic carbon 1s at 284.5 eV and analyzed using CasaXPS (Casa Software Ltd.) peak fitting software. Zirconium 3d spectra (Zr 3d) were numerically fitted with Gaussian-broadened Lorentzian peaks

(GL(50)) after the U2 Tougaard background subtraction with an integrated peak area ratio of 3:2 corresponding to the 3d_{5/2} and 3d_{3/2} states. A full width half maximum (FWHM) of between 1 and 2 eV was allowed during fitting, with an optimal value of 1.75 eV obtained for all Zr 3d spectra; a spin-orbit splitting of 2.4 eV was constrained for each spectrum. Phosphorus 2p spectra (P 2p) were numerically fitted with sets of two Gaussian-broadened Lorentzian peaks (GL(50)) following the Shirley background subtraction, with an integrated peak area ratio of 2:1 corresponding to the 2p_{3/2} and 2p_{1/2} states and a spin-orbit splitting of 0.87 eV. A FWHM of between 1.3 and 2 eV was allowed during initial fitting, with an optimal value of 1.4 eV obtained. The constraints for each species were maintained for the fitting of all XPS spectra acquired during experiments using a constant analyzer pass energy of 71.55 eV.

Temperature-Programmed Desorption/Reaction.

Samples were prepared via a liquid nitrogen matrix deposition (LNMD) method, in which mass-selected (ZrO₂)₃⁻ clusters (4.8×10^{13} clusters, 0.33 clusters/nm²) were deposited into a frozen multilayer matrix of DMMP on the HOPG substrate surface. The LNMD method was inspired by the matrix isolation method developed for infrared spectroscopy,⁶⁶ in which active molecules are trapped within an inactive host matrix, and has been successfully used in this laboratory to study the adsorption and decomposition of DMMP on size-selected (MoO₃)₃ and (WO₃)₃ clusters.^{33,34} The frozen DMMP matrix was prepared by dosing 1 Langmuir (L, 10⁻⁶ Torr s) DMMP ($P_{\text{DMMP}} = 1.0 \times 10^{-8}$ Torr, $\Delta t = 100$ s) onto the LN₂-cooled HOPG substrate (100 K) using the variable leak valve prior to cluster deposition. Temperature programming was accomplished through resistive heating of the HOPG substrate via the current generated by an external power supply (Sorensen DCS 55-55) driven by a programmable PID controller (Eurotherm 2048), resulting in a well-controlled linear temperature ramp (2 K/s). The temperature of the sample throughout TPD/R experiments was measured using a K-type thermocouple spring-loaded to the back side of the HOPG substrate. Following cluster deposition, the sample was heated to 323 K to remove physisorbed DMMP from the HOPG substrate, leaving behind only DMMP chemisorbed to the (ZrO₂)₃ clusters. The prepared, annealed sample was then positioned within several millimeters of the entrance aperture of a line-of-sight quadrupole mass spectrometer (QMS, Hiden HAL/3F PIC), with a built-in electron ionization source and a dedicated secondary electron multiplier pulse-counting detector. The QMS had previously been fitted with a custom-built glass shroud around the electron bombardment ionizer region to minimize noise from residual gas molecules in the chamber during TPD/R experiments. During temperature ramps, the QMS was operated in multiplex mode to simultaneously monitor multiple relevant mass-to-charge (m/z) ratios indicative of any expected volatile species desorbing from the sample surface. For the work reported here, the following masses were measured as a function of sample temperature: $m/z = 16, 29, 30, 31, 32, 46, \text{ and } 79$.

RESULTS AND DISCUSSION

X-ray Photoelectron Spectroscopy. To investigate the effect of increasing temperature on the binding of DMMP to the (ZrO₂)₃ clusters, XPS measurements were taken for a prepared sample at room temperature and after subsequent annealing at successively higher temperatures of 473, 573, and

673 K. In each case, the sample was cooled back down to room temperature prior to each XPS measurement. The uptake of DMMP by the HOPG-supported (ZrO_2)₃ clusters was determined through quantitative analysis of the XPS spectra acquired for each temperature by normalizing the integrated background-subtracted peak areas for the P 2p and Zr 3d regions by the appropriate relative atomic sensitivity factors.⁶⁷ Quantitative determination of the relative amount of zirconium and phosphorus present in the supported cluster sample was feasible in this case due to the size of the (ZrO_2)₃ clusters being much smaller than the inelastic mean free path of the Mg $K\alpha$ X-rays. The resulting ratio of phosphorus to zirconium (P/Zr) in the sample after heating to each temperature is plotted in Figure S1.

At room temperature, the calculated P/Zr value of 0.38 is within 15% of 0.33, which corresponds to one P atom per cluster. While this initially seems to suggest the adsorption of more than one DMMP molecule to some relatively small fraction of the (ZrO_2)₃ clusters, the measured value is also within a reasonable experimental error. Therefore, we estimate that one DMMP molecule was adsorbed per cluster. Moreover, the P/Zr value remains essentially constant within reasonable experimental error over the entire heating range, suggesting no desorption of P-containing species, including molecular DMMP, from the clusters throughout the entire temperature range of this experiment.

The spectra acquired for the Zr 3d region for each annealing temperature are shown in Figure 2.

In the Zr 3d measurements acquired at 298 K, the binding energy for the Zr 3d_{5/2} peak (183.3 eV) is consistent with fully oxidized Zr⁴⁺ reported in the literature for zirconium oxide thin films synthesized via molecular beam epitaxy.^{68–70} After heating to 473 K, the Zr 3d_{5/2} peak was shifted to a slightly higher binding energy (183.5 eV), suggesting further slight oxidation of Zr in some (ZrO_2)₃ clusters. This could be a result of the formation of surface-bound DMMP decomposition product species, that is, methyl methylphosphonate (MMP), methoxy, and methyl phosphonate (MP). Further heating to 573 and 673 K resulted in the Zr 3d_{5/2} peak being shifted back toward a lower binding energy of 183.2 eV. This could be evidence of liberated surface-adsorbed species, such as methoxy. Moreover, the spectra in Figure 2 show no evidence of Zr reduction to oxidation states other than fully oxidized Zr⁴⁺ over the entire heating range, which is in good agreement with the XPS measurements of annealed clean ZrO₂ reported in the literature.⁷¹ Moreover, the lack of any substantial shifts in the Zr 3d spectra acquired across the temperature range suggests no obvious evidence of dramatic changes in the surface morphology of the cluster sample relative to the as-prepared state at room temperature.

The spectra acquired for the P 2p region at each temperature are shown in Figure 3.

Each spectrum exhibited a broad single peak (FWHM ~ 3 eV) with slight asymmetric character. In order to account for the broadness and asymmetry, the peaks were each fitted with a set of P 2p doublets, each corresponding to a distinct P-containing species bound to the clusters. Under the constraints listed in the Experimental Methods section above, optimal fits across all spectra were obtained by incorporating a high energy P 2p doublet (P₁) with a P 2p_{3/2} binding energy of 135.0 eV, and a low energy P 2p doublet (P₂) with a P 2p_{3/2} binding energy of 133.8 eV. These results are similar to XPS measurements previously reported in the literature for

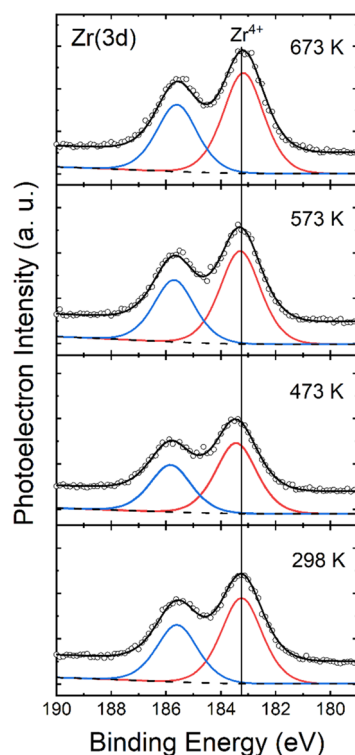


Figure 2. Zr 3d envelope from XPS measurements taken for the HOPG-supported (ZrO_2)₃ clusters with adsorbed DMMP after annealing at the indicated temperatures. The envelope is generated from the fitted doublets corresponding to the Zr 3d_{5/2} (red) and Zr 3d_{3/2} (blue) states. The fitted doublets and background (dashed black line) are offset from the envelope for clarity. The vertical black line marks the Zr 3d_{5/2} peak position at 298 K, assigned to fully oxidized Zr⁴⁺.

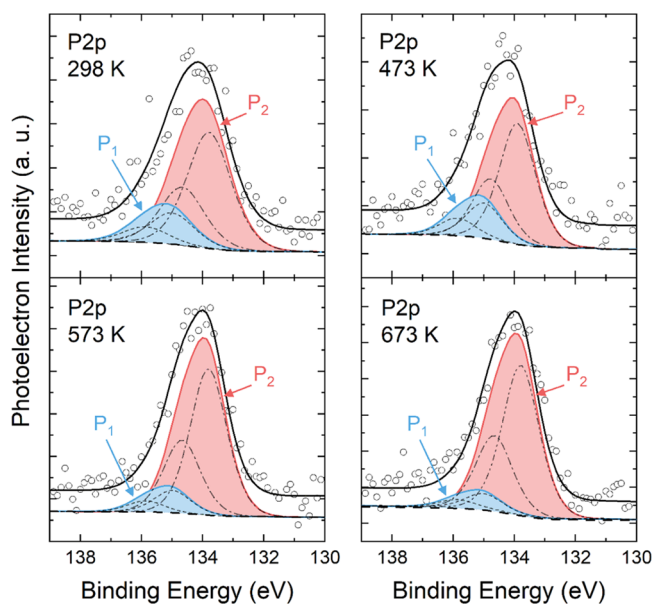


Figure 3. P 2p spectra from XPS measurements taken for the HOPG-supported (ZrO_2)₃ clusters with adsorbed DMMP after annealing at the indicated temperatures. Two discernible P-containing species are present, labeled P₁ (blue) and P₂ (red), with the P 2p_{3/2} and P 2p_{1/2} components for each P 2p peak indicated by dashed and dotted-dashed lines, respectively. The fitted doublets and background (dashed, bold black line) are offset from the envelope for clarity.

DMMP bound to a $\text{TiO}_2(110)$ surface.²³ There, the P 2p XPS spectra were composed of similar high energy (134.9 eV) and low energy (133.7 eV) P 2p doublets, assigned to molecularly chemisorbed DMMP and PO_x species, respectively. Moreover, both the P_1 and P_2 peak doublets have the same FWHM as the single P 2p peak doublet fitted to the XPS spectrum acquired for DMMP molecularly adsorbed to HOPG at 100 K (Figure S2), which exhibited a $2p_{3/2}$ binding energy of 134.2 eV.

In the spectra reported here, similar assignments were made, with P_1 assigned to molecularly adsorbed DMMP and P_2 assigned to P-containing species resulting from DMMP decomposition. At 298 K, the signal for P_2 is larger than that of P_1 by a factor of three, indicating dissociative adsorption of DMMP by the clusters at room temperature. The most commonly observed pathway for DMMP decomposition on metal oxides at and near room temperature is the breaking of a P–OCH₃ bond, resulting in either surface-bound methoxy species, or molecularly adsorbed methanol, depending on the availability of reactive surface species.^{12,17} The resulting P-containing species following P–OCH₃ bond scission generally exhibit a lower P 2p binding energy, due to bonding of the phosphorus center to a lattice oxygen or a surface oxygen stemming from a deprotonated hydroxyl species.²³ This suggests that upon adsorbing to the $(\text{ZrO}_2)_3$ clusters at room temperature, a majority of DMMP readily decomposes.

The integrated peak areas for P_1 and P_2 in each spectrum were calculated and are reported in the accompanying Supporting Information (Table S1), along with the relative percent of each species with respect to the total P 2p signal. The extent of observed DMMP decomposition remains essentially unchanged upon heating to 473 K, according to the P 2p spectrum acquired in Figure 3. Heating to 573 K, resulted in an increase in the intensity of P_2 and a 40% reduction in the intensity of P_1 , indicating further decomposition of adsorbed DMMP after surmounting some thermal barrier between the range of 473 and 573 K. This suggests the existence of two discernible reaction pathways for DMMP decomposition on the $(\text{ZrO}_2)_3$ clusters, that is, a low temperature and high temperature pathway. Finally, heating to 673 K resulted in a continued increase in the intensity of P_2 and an additional 30% reduction in the intensity of P_1 . It is possible that P_2 contains P 2p doublets corresponding to a number of possible P-containing decomposition products, such as MMP and MP, but the lack of higher resolution in the spectra reported in Figure 3 make such further assignments infeasible.

Temperature-Programmed Desorption/Reaction. To investigate the adsorption and reactivity of DMMP on $(\text{ZrO}_2)_3$ clusters, two successive TPD/R experiments were performed. The LNMD method was used for preparing the sample for the first experiment in order to maximize interaction of the clusters with DMMP and mitigate the possibility of post-deposition agglomeration of the clusters on the HOPG substrate. After preparing the sample, the substrate temperature was initially ramped to 323 K to remove the frozen DMMP multilayer and any remaining physisorbed DMMP. A TPD spectrum showing the physi-desorption of DMMP, acquired for DMMP adsorbed on bare HOPG, is shown in the accompanying Supporting Information (Figure S3). After removing the physisorbed DMMP, a TPD/R spectrum was acquired over a temperature range of 323–723 K, the results of which are shown in Figure 4.

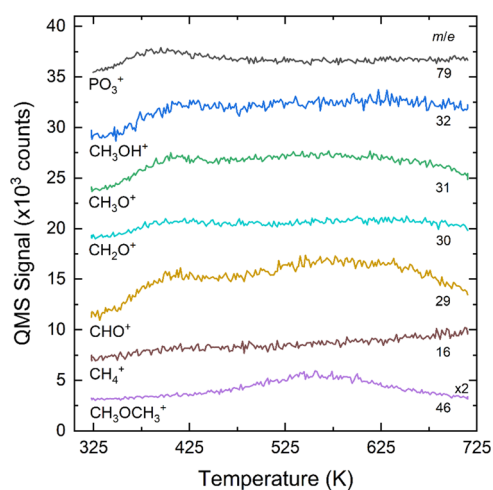


Figure 4. As-acquired TPD/R spectrum for DMMP adsorbed to $(\text{ZrO}_2)_3$ clusters, prepared via an LNMD method, with each mass trace labeled by measured m/z value and assigned molecular ion fragment. m/z traces are vertically offset from each other for clarity.

The molecular desorption of intact DMMP is indicated by $m/z = 79$, which is a major fragment in a typical electron impact (EI) ionization mass spectrum of DMMP. Interestingly, here, the signal for 79 is weaker than other product fragments measured (i.e., $m/z = 32$, 31, and 29). Based on the peak position and signal intensity, it is possible that the molecular desorption peak observed here for DMMP originates from the bare HOPG surface or sample holder assembly, as typical background TPD experiments for DMMP exhibit largely the same result. This interpretation is bolstered by the fact that XPS measurements showed fairly high uptake of DMMP at room temperature, with virtually no change in the relative amount of phosphorus-containing species adsorbed to the clusters up to 673 K. These results taken together suggest a very low molecular desorption propensity for DMMP from the $(\text{ZrO}_2)_3$ clusters following initial adsorption.

Determining the identity of any desorbing species resulting from DMMP decomposition on the clusters requires an analysis accounting for the cracking pattern of molecularly desorbed DMMP and any decomposition products, in this case dimethyl ether, methanol, and formaldehyde. Contributions of molecularly desorbed DMMP to the signals measured for $m/z = 32$, 31, 30, and 29 must be determined and subtracted to reveal the signal in the TPD/R spectrum arising solely from other desorbing species. For DMMP, this involved the cracking pattern obtained from the dose profile of a sufficiently prepared, clean DMMP sample dose and a typical background TPD spectrum measured for a frozen multilayer of DMMP on HOPG in our system. These spectra (Figure S4) and details of the cracking analysis are reported in the accompanying Supporting Information. The results, shown in Figure 5, reveal the volatile DMMP decomposition products that were desorbed during the TPD/R experiment. Here, desorption of methanol, formaldehyde, and dimethyl ether is indicated by the traces measured for $m/z = 31$, 29, and 46, respectively, where 31 has been adjusted for contribution from DMMP desorption and 29 has been adjusted for contribution from DMMP, methanol, and dimethyl ether desorption.

The results illustrated in Figure 5 indicate that methanol is the major desorption product resulting from DMMP decomposition on the $(\text{ZrO}_2)_3$ clusters, while formaldehyde

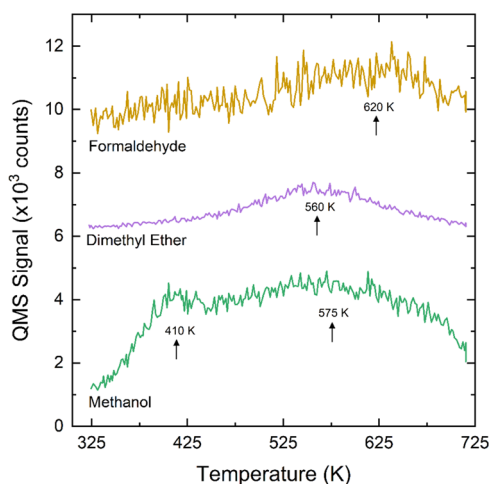


Figure 5. Desorption profiles of volatile decomposition products, methanol ($m/z = 31$), dimethyl ether ($m/z = 46$), and formaldehyde ($m/z = 29$) measured during TPD/R of DMMP adsorbed to $(\text{ZrO}_2)_3$ clusters, following correction for the cracking patterns of desorbing molecular species. Approximate desorption peak positions are labeled by an arrow and corresponding temperature. m/z traces are vertically offset from each other for clarity.

and dimethyl ether appear to be relatively minor decomposition products, which can form via reaction pathways that become accessible at higher temperatures. The peak desorption temperature for each product was assigned by comparing the major fragment traces with those of the other relevant cracking fragment(s) for the respective desorption product. Methanol desorption is clearly manifested in two distinct peaks at different temperatures, that is, a low temperature peak around 410 K and a high temperature peak around 575 K. Dimethyl ether desorption showed a single peak around 560 K, while formaldehyde desorption showed a single peak around 620 K. The broadness of the peaks observed here are to be expected for experiments involving subnanoscale clusters supported by a substrate surface. Even if the native geometries of the clusters are maintained after soft-landing onto the surface, the subsequent temperature ramp during the experiments will provide enough energy to the clusters to allow them to access a statistical ensemble of possible states.⁷² The resulting chemistry, evidenced via product desorption, will thereby reflect the ensemble average of these many states, and its dynamic evolution throughout the reaction cycle. Additional complicating factors, including adsorbate-induced changes to the cluster geometries resulting from DMMP chemisorption and ensuing decomposition chemistry, can be expected to further expand the landscape of present structures contributing to measured signal. Such phenomena have been predicted through rigorous theoretical treatments^{73,74} and supported by experiments⁷⁵ performed by others studying the chemistry of surface-supported clusters.

Moreover, given that the $(\text{ZrO}_2)_3$ clusters are small and HOPG exhibits a fairly weak cluster–support interaction relative to other substrates, it is likely that the clusters can become mobilized and diffuse across the support at elevated temperatures. Indeed, this phenomenon has been observed in studies of various clusters on HOPG, the majority of which have involved metal clusters deposited via physical vapor methods. It has been shown that small metal clusters may become mobilized and diffuse across a pristine HOPG surface

above cryogenic temperatures,⁷⁶ and coalescence into much larger particles can occur as a result of high temperature annealing,⁷⁷ and even room temperature treatment.^{78,79} HOPG surfaces with high defect density, typically achieved via soft Ar^+ ion sputtering, have been found to exacerbate coalescence or ripening of small clusters into larger particles even further.^{77,80}

This phenomenon motivated earlier works in our laboratory, which compared the surface morphology of samples prepared by soft-landing two different species of mass-selected clusters onto pristine HOPG, namely, either $\text{Mo}_{100\pm 2.5}^-$ or $(\text{MoO}_3)_{67\pm 1.5}^-$.⁶⁵ These clusters, having the same nominal mass, were chosen to investigate whether different behavior was observed for deposited metallic versus oxide clusters of the same metal. At a submonolayer coverage, with a substrate preparation temperature of 298 K, in situ STM imaging showed the metallic Mo clusters had preferentially organized along step edges, whereas the MoO_3 clusters were stochastically distributed across terraces. This suggested that the deposited oxide clusters were less prone to diffusion across the HOPG surface following deposition. In another related study in our laboratory, small $(\text{WO}_3)_3^-$ clusters were soft-landed at submonolayer coverage onto pristine HOPG maintained at 100 K. Ex situ atomic force microscopy measurements, following atmosphere exposure during sample transfer, showed two-dimensional, ramified fractal-like assemblies, which persisted even after annealing at 673 K.⁸¹ Taken together, these two studies show that metal oxide clusters supported on HOPG, even very small clusters, can exhibit a much lower propensity for diffusion and coalescence into large three-dimensional particles, such as that seen for various metal clusters supported on HOPG. However, while great care was taken to ensure interaction of monodisperse $(\text{ZrO}_2)_3$ clusters with DMMP, at the elevated temperatures during annealing treatments between XPS measurements and the linear temperature ramp during TPD/R experiments, some extent of cluster agglomeration cannot be ruled out and may even contribute to desorption signal broadening and loss of reactivity on subsequent DMMP exposure.

Regarding methanol desorption shown in Figure 5, the low temperature peak is of similar intensity to the high temperature peak, but its profile is much narrower, while the high temperature peak is rather broad. It has been well established by previous studies in the literature that methanol production via DMMP decomposition on metal oxide surfaces is the result of protonation of a methoxy species often arising from P–OCH₃ bond cleavage by either surface bound water or surface hydroxyls. Direct evidence has been found for this mechanism in studies of amorphous $\text{Zr}(\text{OH})_4$ thin films and DMMP,^{43,44} as well as mesoporous zirconium hydr(oxide), that is, $\text{ZrO}_2/\text{Zr}(\text{OH})_4$, and a reactive nerve agent simulant, dimethyl chlorophosphate.⁸² Even in the UHV environment used for the studies in this work, surface-bound water and surface hydroxyls may be present to some degree on the clusters,⁸³ allowing for the generation of methanol from methoxy species resulting from DMMP decomposition. Indeed, a previous study of the adsorption and decomposition of DMMP on size-selected molybdenum oxide clusters supported on HOPG performed in our laboratory, supplemented by calculations from theoretical collaborators, supported this claim.³³

The presence of two distinct desorption peaks suggests either the existence of two distinct binding states for the bound methoxy species, or two energetically different pathways for

generating bound methoxies from DMMP decomposition on the clusters. While there has been virtually no published work investigating the adsorption and decomposition of DMMP by subnanoscale ZrO_2 , that is, small clusters, previous experiments by Gordon have shown strong evidence for the effective adsorption and decomposition of DMMP by small zirconium oxide nanoparticles (1.6 ± 0.9 and 1.9 ± 0.9 nm) at room temperature in a UHV environment, despite the relative inactivity of bulk crystalline ZrO_2 for DMMP decomposition.⁴⁹ Through in situ Fourier-transform infrared spectroscopy studies, strong evidence was found for the adsorption of DMMP and subsequent facile elimination of a methoxy group resulting in an O–P–O bridging bound MMP species and a surface-bound methoxy. Coupled with the fact that chemisorbed methanol has been found to desorb molecularly from a hydroxylated ZrO_2 powder catalyst near 400 K,⁸⁴ this suggests that the low temperature methanol peak corresponds to the desorption of methanol formed via protonation of methoxies resulting from a single decomposition step in which a P–OCH₃ bond of DMMP is broken to form bound MMP and methoxy. Then, as the temperature is increased, further decomposition of DMMP, generating MP and additional methoxy species, could be subsequently protonated to methanol which could immediately desorb, generating the high temperature broad desorption peak.

While the TPD/R results indicate that methanol is the dominant volatile product formed via DMMP decomposition on the clusters, other pathways are clearly accessed at higher temperatures. Bulk ZrO_2 has been shown to exhibit both acidic and basic character, motivating its designation as a “redox catalyst” by Wachs et al. in an expansive characterization of the surface reactivity of a host of metal oxides.⁸⁵ Their experiments involving exposure of bulk ZrO_2 to methanol, used as a “smart probe” of surface active sites, showed the formation of primarily formaldehyde and methyl formate at a temperature of around 600 K. Moreover, surface methoxies, which are present on the clusters resulting from P–OCH₃ bond scission of DMMP prior to protonation and methanol evolution, are known to be the intermediates in the formation of formaldehyde and dimethyl ether as well.⁸⁶ A study of several acidic metal oxide catalysts found that the reaction of methanol to dimethyl ether preferred weak to medium acid sites, while the formation of methane preferred strong acid sites.⁸⁷ Notably, we observe no methane formation, which seems to be in line with ZrO_2 exhibiting redox catalyst characteristics with an intermediate acidic nature, as opposed to being a strong acid catalyst. In general, methanol to dimethyl ether activity has been demonstrated to correlate positively with catalyst acid strength for a wide range of bulk and supported metal oxides.^{88,89} In fact, methanol exposure on a ZrO_2 aerogel has been found to produce dimethyl ether at elevated temperatures.⁹⁰ In the case of our experiment, it is possible that dimethyl ether formation occurs via the interaction of either methanol resulting from DMMP decomposition or a surface methoxy with a P–OCH₃ species on a cluster-bound phosphonate. In a recent rigorous study involving the decomposition of DMMP on a well-defined Fe_3O_4 (111) surface in UHV, it was convincingly demonstrated via isotopic labeling and accompanying DFT calculations that dimethyl ether formation at around 600 K during TPD/R experiments was solely due to intramolecular reaction of surface-bound MMP species, complicating this picture even further.⁹¹ That work also demonstrated that oxygen adatoms on the surface,

that is, undercoordinated oxygen atoms, are key to the observed DMMP decomposition pathways.

The decomposition of surface methoxy species on bulk ZrO_2 crystal surfaces has been shown to be highly dependent on the crystal plane identity of the surface. In particular, the (110) surface is active for the formation of a dioxymethylene surface intermediate that can give rise to formaldehyde desorption at elevated temperatures above 450 K, while the (100) surface exhibits no formaldehyde production.⁹² This is attributed to the presence of undercoordinated oxygen species present in the (110) surface, species the likes of which are expected to be present on a $(\text{ZrO}_2)_3$ cluster. Hence, the high temperature evolution of formaldehyde observed in our TPD/R experiment is most likely due to the oxidation of a second methoxy liberated from a MMP surface intermediate, having already lost a methoxy, which had most likely been protonated to form methanol. To our knowledge, all the experimental studies of DMMP decomposition via Zr-containing materials published to-date have only reported the evolution of methanol as a volatile reaction product. The observation here of formaldehyde and dimethyl ether evolution resulting from DMMP decomposition suggests that other volatile product species may be formed on these materials as well. This result seems to support a prediction made in a recent theoretical study on the hydrolysis of DMMP by a $\text{Zr}_4(\text{OH})_{16}$ cluster, which can be viewed as a fully hydroxylated close relative to our HOPG-supported $(\text{ZrO}_2)_3$ clusters.⁹³ The DFT calculations performed showed that methanol formation via an addition–elimination mechanism was the most energetically favorable reaction pathway, resulting in a monodentate cluster-bound MMP species that could potentially undergo further decomposition prior to forming a more stable bridging-type intermediate. While our experiments do not prove such a mechanism, the observation of additional high-temperature reaction products that are characteristic of DMMP decomposition are highly suggestive. Future investigations should pay especially close attention to the possibility of such chemistry occurring, especially under conditions where the concentration of surface hydroxyls can be depleted.

To investigate the potential activity of the $(\text{ZrO}_2)_3$ clusters on subsequent exposures of DMMP, a second TPD/R experiment was performed on the same sample immediately following the experiment illustrated in Figures 4 and 5. After completing the temperature ramp for the first TPD/R experiment, the sample was cooled back down to 100 K and exposed to a 2 L system dose of DMMP. The sample was then heated to 323 K to remove the physisorbed DMMP, followed by the collection of a TPD/R spectrum, the results of which are shown in Figure 6.

Upon inspection, the second TPD/R spectrum appears to only show evidence of molecular DMMP desorption. The relative intensities of the species shown in the spectrum correspond quite well to that of the typical background TPD for DMMP on bare HOPG (Figure S4). The DMMP desorption peak in this case has shifted lower to 373 K but is still within the range of observed DMMP desorption peak positions in background TPD experiments. To further confirm this suspicion, the second TPD/R experiment data were analyzed based on expected cracking patterns and DMMP background TPD observations as described previously, the results of which are shown in Figure 7.

After accounting for the DMMP background desorption from HOPG and the sample holder assembly and expected

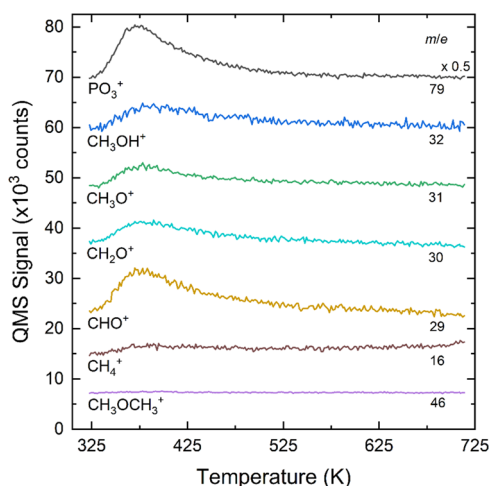


Figure 6. As-acquired TPD/R spectra for DMMP dosed at 100 K onto residual HOPG-supported $(\text{ZrO}_2)_3$ clusters after one previous TPD/R cycle, with each mass trace labeled by measured m/z value and assigned molecular ion fragment. m/z traces are vertically offset from each other for clarity.

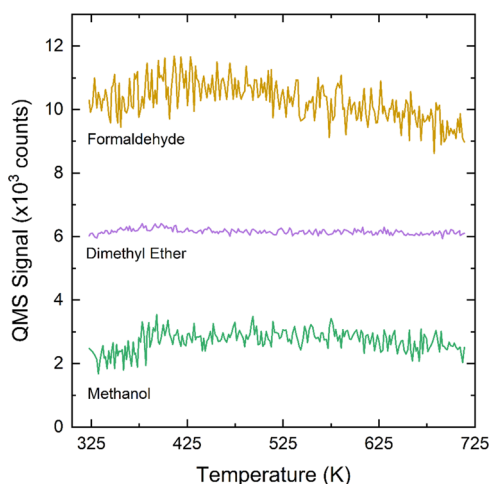


Figure 7. Desorption profiles of methanol ($m/z = 31$), dimethyl ether ($m/z = 46$), and formaldehyde ($m/z = 29$) measured for a second TPD/R cycle of DMMP on post-reaction HOPG-supported $(\text{ZrO}_2)_3$ clusters, following correction for the cracking patterns of desorbing molecular species. m/z traces are vertically offset from each other for clarity.

cracking patterns of any desorbing species, it is clear that no discernible evidence of the decomposition products observed during the first TPD/R experiment manifest here. This result is in agreement with the XPS measurements which suggested the retention of cluster-bound phosphorus-containing species up to at least a temperature of 673 K, which likely poison the cluster active site(s) and prevent subsequent chemisorption and decomposition of DMMP. Hence, while the $(\text{ZrO}_2)_3$ clusters show promising evidence of a high propensity for DMMP adsorption and facile activity toward DMMP decomposition, likely owing to the presence of hydroxyl species, it appears that the observed decomposition chemistry is stoichiometric rather than catalytic.

This is unsurprising, as the deactivation due to irreversible adsorption of P-containing decomposition products of DMMP has been widely observed for a wide variety of metal oxide materials, including the most promising Zr-containing species

to-date. Zr-based MOFs, typically used to decompose DMMP hydrolytically in buffered aqueous solution, generally show irreversible binding of P-containing products to the nodal active site.⁹⁴ A combined experimental/theoretical study of Zr_6 -based MOFs exposed to DMMP in UHV likewise showed an irreversible binding of P-containing products after heating to 600 K, which inhibited further DMMP decomposition.⁶⁰ $\text{Zr}(\text{OH})_4$ thin films, which have been found to decompose DMMP very effectively to evolve methanol, are also poisoned due to the irreversible binding of P-containing products, even after thermal treatment at 673 K.⁴³ The same was observed for ZrO_2 -based hydroxylated aerogels, which effectively decomposed DMMP at room temperature.⁹⁵ While this seemingly universal problem of strong binding and retention of P-containing species to the active sites of a model organophosphate decomposition material can prevent true catalytic performance, it does not entirely undermine the function of a candidate protective material. The strong binding of organophosphonate species and their decomposition products by previously studied Zr-containing materials, shown here to hold true for $(\text{ZrO}_2)_3$ clusters at the small-size limit of ZrO_2 -based species, is still a crucial property for any material intended for the use of personal protection against CWAs.

CONCLUSIONS

The nature of the adsorption and decomposition of DMMP on size-selected $(\text{ZrO}_2)_3$ clusters supported on HOPG has been explored via a combination of XPS and TPD/R experiments. DMMP simultaneously dosed during cluster deposition was adsorbed at an approximately one-to-one ratio by the clusters at room temperature, and the uptake of DMMP by the clusters persisted upon heating to as high as 673 K. DMMP decomposition was observed on a majority of the clusters at room temperature, likely via a P–OCH₃ bond scission, resulting in the formation of bound MMP and methoxy species. Upon heating to 410 K, the bound methoxies were protonated, likely by nearby hydroxyl species, to form methanol which could readily desorb from the clusters. At temperatures above 473 K, an alternative series of DMMP decomposition pathways was accessed, resulting in the additional formation of methanol, along with dimethyl ether and formaldehyde. This diversity of reaction pathways has not been previously demonstrated for reported experimental studies of hydroxylated zirconium materials, which to-date have shown especially promising results for DMMP and nerve agent decomposition. This suggests the decomposition chemistry on these materials may be more complex than has been demonstrated thus far. Exposure of the reacted clusters to a subsequent cycle of DMMP dosing and TPD/R resulted in molecular DMMP desorption, with no detectable formation of the previously observed reaction products. Hence, one DMMP reaction cycle up to as high as 723 K effectively poisoned the clusters, drastically inhibiting their adsorption and decomposition characteristics upon subsequent exposure, but showing high retention of P-containing toxic product species.

ASSOCIATED CONTENT

Supporting Information

The Supporting Information is available free of charge at <https://pubs.acs.org/doi/10.1021/acs.jpcc.1c06063>.

Relative atomic ratio of phosphorus to zirconium at various temperatures, quantification and comparison of

P 2p XPS component peaks at various temperatures, P 2p XPS spectrum and TPD spectrum for DMMP frozen matrix on bare HOPG at 100 K, and description of cracking analysis for species desorbed during TPD/R experiment (PDF)

AUTHOR INFORMATION

Corresponding Author

Kit H. Bowen – Department of Chemistry, Johns Hopkins University, Baltimore, Maryland 21218, United States; orcid.org/0000-0002-2858-6352; Email: kbowen@jhu.edu

Authors

Michael A. Denchy – Department of Chemistry, Johns Hopkins University, Baltimore, Maryland 21218, United States; orcid.org/0000-0002-2757-8705

Linjie Wang – Department of Chemistry, Johns Hopkins University, Baltimore, Maryland 21218, United States; orcid.org/0000-0002-6558-1753

Nicolas Blando – Department of Chemistry, Johns Hopkins University, Baltimore, Maryland 21218, United States

Lucas Hansen – Department of Chemistry, Johns Hopkins University, Baltimore, Maryland 21218, United States

Benjamin R. Bilik – Department of Chemistry, Johns Hopkins University, Baltimore, Maryland 21218, United States

Xin Tang – Department of Chemistry, Johns Hopkins University, Baltimore, Maryland 21218, United States

Zachary Hicks – Department of Chemistry, Johns Hopkins University, Baltimore, Maryland 21218, United States

Gerd Gantefer – Fachbereich Fuer Physik, Universitaet Konstanz, 78457 Konstanz, Germany

Complete contact information is available at: <https://pubs.acs.org/10.1021/acs.jpcc.1c06063>

Notes

The authors declare no competing financial interest.

ACKNOWLEDGMENTS

This material is based upon work supported by the Defense Threat Reduction Agency (DTRA) under grant number HDTRA11510005 and the Army Research Office (ARO) under grant number W911NF2020207.

REFERENCES

- (1) Munro, N.; Ambrose, K. R.; Watson, A. P. Toxicity of the Organophosphate Chemical Warfare Agents GA, GB, and VX: Implications for Public Protection. *Environ. Health Perspect.* **1994**, *102*, 18–37.
- (2) Kim, K.; Tsay, O. G.; Atwood, D. A.; Churchill, D. G. Destruction and Detection of Chemical Warfare Agents. *Chem. Rev.* **2011**, *111*, 5345–5403.
- (3) Yang, Y. C.; Baker, J. A.; Ward, J. R. Decontamination of Chemical Warfare Agents. *Chem. Rev.* **1992**, *92*, 1729–1743.
- (4) Ekerdt, J. G.; Klabunde, K. J.; Shapley, J. R.; White, J. M.; Yates, J. T. Surface Chemistry of Organophosphorus Compounds. *J. Phys. Chem.* **1988**, *92*, 6182–6188.
- (5) Park, S. H.; McClain, S.; Tian, Z. R.; Suib, S. L.; Karwacki, C. Surface and Bulk Measurements of Metals Deposited on Activated Carbon. *Chem. Mater.* **1997**, *9*, 176–183.
- (6) Morrison, R. W. *NBC Filter Performance; U.S. Army Soldier and Biological Chemical Command; Aberdeen Proving Ground: MD*, 2001.

(7) Hegde, R. I.; Greenleaf, C. M.; White, J. M. Surface chemistry of dimethyl methylphosphonate on rhodium(100). *J. Phys. Chem.* **1985**, *89*, 2886–2891.

(8) Henderson, M. A.; White, J. M. Adsorption and Decomposition of Dimethyl Methylphosphonate on Platinum(111). *J. Am. Chem. Soc.* **1988**, *110*, 6939–6947.

(9) Smentkowski, V. S.; Hagans, P.; Yates, J. T. Study of the Catalytic Destruction of Dimethyl Methylphosphonate: Oxidation over Mo(110). *J. Phys. Chem.* **1988**, *92*, 6351–6357.

(10) Guo, X.; Yoshinobu, J.; Yates, J. T. Decomposition of an Organophosphonate Compound (Dimethyl Methylphosphonate) on the Ni(111) and Pd(111) Surfaces. Decomposition of an organophosphonate compound (dimethylmethylphosphonate) on the nickel(111) and palladium(111) surfaces. *J. Phys. Chem.* **1990**, *94*, 6839–6842.

(11) Templeton, M. K.; Weinberg, W. H. Adsorption and Decomposition of Dimethyl Methylphosphonate on an Aluminum Oxide Surface. *J. Am. Chem. Soc.* **1985**, *107*, 97–108.

(12) Aurian-Blajeni, B.; Boucher, M. M. Interaction of Dimethyl Methylphosphonate with Metal Oxides. *Langmuir* **1989**, *5*, 170–174.

(13) Trotochaud, L.; Head, A. R.; Büchner, C.; Yu, Y.; Karslıoğlu, O.; Tsyshevsky, R.; Holdren, S.; Eichhorn, B.; Kuklja, M. M.; Bluhm, H. Room Temperature Decomposition of Dimethyl Methylphosphonate on Cuprous Oxide Yields Atomic Phosphorus. *Surf. Sci.* **2019**, *680*, 75–87.

(14) Trotochaud, L.; Tsyshevsky, R.; Holdren, S.; Fears, K.; Head, A. R.; Yu, Y.; Karslıoğlu, O.; Pletincx, S.; Eichhorn, B.; Owrutsky, J.; et al. Spectroscopic and Computational Investigation of Room-Temperature Decomposition of a Chemical Warfare Agent Simulant on Polycrystalline Cupric Oxide. *Chem. Mater.* **2017**, *29*, 7483–7496.

(15) Henderson, M. A.; Jin, T.; White, J. M. A TPD/AES Study of the Interaction of Dimethyl Methylphosphonate with Iron Oxide α -Fe₂O₃ and SiO₂. *J. Phys. Chem.* **1986**, *90*, 4607–4611.

(16) Hegde, R. I.; White, J. M. Interaction of Dimethyl Methylphosphonate with Oxidized Iron and the Effect of Coadsorbed Water. *Appl. Surf. Sci.* **1987**, *28*, 1–10.

(17) Mitchell, M. B.; Sheinker, V. N.; Mintz, E. A. Adsorption and Decomposition of Dimethyl Methylphosphonate on Metal Oxides. *J. Phys. Chem. B* **1997**, *101*, 11192–11203.

(18) Segal, S. R.; Cao, L.; Suib, S. L.; Tang, X.; Satyapal, S. Thermal Decomposition of Dimethyl Methylphosphonate over Manganese Oxide Catalysts. *J. Catal.* **2001**, *198*, 66–76.

(19) Head, A. R.; Tsyshevsky, R.; Trotochaud, L.; Yu, Y.; Kyhl, L.; Karslıoğlu, O.; Kuklja, M. M.; Bluhm, H. Adsorption of Dimethyl Methylphosphonate on MoO₃: The Role of Oxygen Vacancies. *J. Phys. Chem. C* **2016**, *120*, 29077–29088.

(20) Head, A. R.; Tang, X.; Hicks, Z.; Wang, L.; Bleuel, H.; Holdren, S.; Trotochaud, L.; Yu, Y.; Kyhl, L.; Karslıoğlu, O.; et al. Thermal Desorption of Dimethyl Methylphosphonate from MoO₃. *Catal., Struct. React.* **2017**, *3*, 112–118.

(21) Rusu, C. N.; Yates, J. T. Adsorption and Decomposition of Dimethyl Methylphosphonate on TiO₂. *J. Phys. Chem. B* **2000**, *104*, 12292–12298.

(22) Kim, C. S.; Lad, R. J.; Tripp, C. P. Interaction of Organophosphorous Compounds with TiO₂ and WO₃ Surfaces Probed by Vibrational Spectroscopy. *Sens. Actuators, B* **2001**, *76*, 442–448.

(23) Zhou, J.; Varazo, K.; Reddic, J. E.; Myrick, M. L.; Chen, D. A. Decomposition of Dimethyl Methylphosphonate on TiO₂(110): Principal Component Analysis Applied to X-Ray Photoelectron Spectroscopy. *Anal. Chim. Acta* **2003**, *496*, 289–300.

(24) Trubitsyn, D. A.; Vorontsov, A. V. Experimental Study of Dimethyl Methylphosphonate Decomposition over Anatase TiO₂. *J. Phys. Chem. B* **2005**, *109*, 21884–21892.

(25) Kanan, S. M.; Lu, Z.; Tripp, C. P. A Comparative Study of the Adsorption of Chloro- and Non-Chloro-Containing Organophosphorus Compounds on WO₃. *J. Phys. Chem. B* **2002**, *106*, 9576–9580.

(26) Verma, M.; Chandra, R.; Gupta, V. K. Decontamination of 2-Chloro Ethyl Sulphide and Dimethyl Methyl Phosphonate from

Aqueous Solutions Using Manganese Oxide Nanostructures. *J. Mol. Liq.* **2016**, *215*, 285–292.

(27) Št'astný, M.; Tolasz, J.; Štengl, V.; Henych, J.; Žižka, D. Graphene Oxide/MnO₂ Nanocomposite as Destructive Adsorbent of Nerve-Agent Simulants in Aqueous Media. *Appl. Surf. Sci.* **2017**, *412*, 19–28.

(28) Gordon, W. O.; Tissue, B. M.; Morris, J. R. Adsorption and Decomposition of Dimethyl Methylphosphonate on Y₂O₃ Nanoparticles. *J. Phys. Chem. C* **2007**, *111*, 3233–3240.

(29) Bisio, C.; Carniato, F.; Palumbo, C.; Safronyuk, S. L.; Starodub, M. F.; Katsev, A. M.; Marchese, L.; Guidotti, M. Nanosized Inorganic Metal Oxides as Heterogeneous Catalysts for the Degradation of Chemical Warfare Agents. *Catal. Today* **2016**, *277*, 192–199.

(30) Ma, S.; Zhou, J.; Kang, Y. C.; Reddic, J. E.; Chen, D. A. Dimethyl Methylphosphonate Decomposition on Cu Surfaces: Supported Cu Nanoclusters and Films on TiO₂(110). *Langmuir* **2004**, *20*, 9686–9694.

(31) Zhou, J.; Ma, S.; Kang, Y. C.; Chen, D. A. Dimethyl Methylphosphonate Decomposition on Titania-Supported Ni Clusters and Films: A Comparison of Chemical Activity on Different Ni Surfaces. *J. Phys. Chem. A* **2004**, *108*, 11633–11644.

(32) Ratliff, J. S.; Tenney, S. A.; Hu, X.; Conner, S. F.; Ma, S.; Chen, D. A. Decomposition of Dimethyl Methylphosphonate on Pt, Au, and Au-Pt Clusters Supported on TiO₂(110). *Langmuir* **2009**, *25*, 216–225.

(33) Tang, X.; Hicks, Z.; Wang, L.; Ganteför, G.; Bowen, K. H.; Tsyshkevsky, R.; Sun, J.; Kuklja, M. M. Adsorption and Decomposition of Dimethyl Methylphosphonate on Size-Selected (MoO₃)₃ Clusters. *Phys. Chem. Chem. Phys.* **2018**, *20*, 4840–4850.

(34) Tang, X.; Hicks, Z.; Ganteför, G.; Eichhorn, B. W.; Bowen, K. H. Adsorption and Decomposition of DMMP on Size-Selected (WO₃)₃ Clusters. *ChemistrySelect* **2018**, *3*, 3718–3721.

(35) Peterson, G. W.; Karwacki, C. J.; Feaver, W. B.; Rossin, J. A. Zirconium Hydroxide as a Reactive Substrate for the Removal of Sulfur Dioxide. *Ind. Eng. Chem. Res.* **2009**, *48*, 1694–1698.

(36) Seredych, M.; Bandoz, T. J. Effects of Surface Features on Adsorption of SO₂ on Graphite Oxide/Zr(OH)₄ Composites. *J. Phys. Chem. C* **2010**, *114*, 14552–14560.

(37) Peterson, G. W.; Wagner, G. W.; Keller, J. H.; Rossin, J. A. Enhanced Cyanogen Chloride Removal by the Reactive Zirconium Hydroxide Substrate. *Ind. Eng. Chem. Res.* **2010**, *49*, 11182–11187.

(38) Bandoz, T. J.; Laskoski, M.; Mahle, J.; Mogilevsky, G.; Peterson, G. W.; Rossin, J. A.; Wagner, G. W. Reactions of VX, GD, and HD with Zr(OH)₄: Near Instantaneous Decontamination of VX. *J. Phys. Chem. C* **2012**, *116*, 11606–11614.

(39) Giannakoudakis, D. A.; Mitchell, J. K.; Bandoz, T. J. Reactive Adsorption of Mustard Gas Surrogate on Zirconium (Hydr)Oxide/Graphite Oxide Composites: The Role of Surface and Chemical Features. *J. Mater. Chem. A* **2016**, *4*, 1008–1019.

(40) Astle, M. A.; Rance, G. A.; Fay, M. W.; Notman, S.; Sambrook, M. R.; Khlobystov, A. N. Synthesis of Hydroxylated Group IV Metal Oxides inside Hollow Graphitized Carbon Nanofibers: Nano-Sponges and Nanoreactors for Enhanced Decontamination of Organophosphates. *J. Mater. Chem.* **2018**, *6*, 20444–20453.

(41) Kim, S.; Ying, W. B.; Jung, H.; Ryu, S. G.; Lee, B.; Lee, K. J. Zirconium Hydroxide-Coated Nanofiber Mats for Nerve Agent Decontamination. *Chem.—Asian J.* **2017**, *12*, 698–705.

(42) Balow, R. B.; Lundin, J. G.; Daniels, G. C.; Gordon, W. O.; Mcentee, M.; Peterson, G. W.; Wynne, J. H.; Pehrsson, P. E. Environmental Effects on Zirconium Hydroxide Nanoparticles and Chemical Warfare Agent Decomposition: Implications of Atmospheric Water and Carbon Dioxide. *ACS Appl. Mater. Interfaces* **2017**, *9*, 39747–39757.

(43) Jeon, S.; Balow, R. B.; Daniels, G. C.; Ko, J. S.; Pehrsson, P. E. Conformal Nanoscale Zirconium Hydroxide Films for Decomposing Chemical Warfare Agents. *Appl. Nano Mater.* **2019**, *2*, 2295–2307.

(44) Jeon, S.; Schweigert, I. V.; Pehrsson, P. E.; Balow, R. B. Kinetics of Dimethyl Methylphosphonate Adsorption and Decomposition on Zirconium Hydroxide Using Variable Temperature In Situ Attenuated

Total Reflection Infrared Spectroscopy. *ACS Appl. Mater. Interfaces* **2020**, *12*, 14662–14671.

(45) Tanabe, K. Surface and Catalytic Properties of ZrO₂. *Mater. Chem. Phys.* **1985**, *13*, 347–364.

(46) Bensitel, M.; Saur, O.; Lavalley, J. C.; Mabilon, G. Acidity of Zirconium Oxide and Sulfated ZrO₂ Samples. *Mater. Chem. Phys.* **1987**, *17*, 249–258.

(47) Haruta, M. Size- and Support-Dependency in the Catalysis of Gold. *Catal. Today* **1997**, *36*, 153–166.

(48) Sanchez, A.; Abbet, S.; Heiz, U.; Schneider, W.-D.; Häkkinen, H.; Barnett, R. N.; Landman, U. When Gold Is Not Noble: Nanoscale Gold Catalysts. *J. Phys. Chem. A* **1999**, *103*, 9573–9578.

(49) Gordon, W. O. Metal Oxide Nanoparticles: Optical Properties and Interaction with Chemical Warfare Agent Simulants. Ph.D. Dissertation, Virginia Polytechnic Institute and State University, Blacksburg, VA, 2006.

(50) Katz, M. J.; Moon, S.-Y.; Mondloch, J. E.; Beyzavi, M. H.; Stephenson, C. J.; Hupp, J. T.; Farha, O. K. Exploiting Parameter Space in MOFs: A 20-Fold Enhancement of Phosphate-Ester Hydrolysis with UiO-66-NH₂. *Chem. Sci.* **2015**, *6*, 2286–2291.

(51) Moon, S.-Y.; Wagner, G. W.; Mondloch, J. E.; Peterson, G. W.; DeCoste, J. B.; Hupp, J. T.; Farha, O. K. Effective, Facile, and Selective Hydrolysis of the Chemical Warfare Agent VX Using Zr₆-Based Metal-Organic Frameworks. *Inorg. Chem.* **2015**, *54*, 10829–10833.

(52) Mondloch, J. E.; Katz, M. J.; Isley III, W. C.; Ghosh, P.; Liao, P.; Bury, W.; Wagner, G. W.; Hall, M. G.; Decoste, J. B.; Peterson, G. W.; et al. Destruction of Chemical Warfare Agents Using Metal-Organic Frameworks. *Nat. Mater.* **2015**, *14*, 512–516.

(53) Moon, S.-Y.; Liu, Y.; Hupp, J. T.; Farha, O. K. Instantaneous Hydrolysis of Nerve-Agent Simulants with a Six-Connected Zirconium-Based Metal-Organic Framework. *Angew. Chem., Int. Ed.* **2015**, *54*, 6795–6799.

(54) Li, P.; Klet, R. C.; Moon, S.-Y.; Wang, T. C.; Deria, P.; Peters, A. W.; Klahr, B. M.; Park, H.-J.; Al-Juaied, S. S.; Hupp, J. T.; et al. Synthesis of Nanocrystals of Zr-Based Metal-Organic Frameworks with Csq-Net: Significant Enhancement in the Degradation of a Nerve Agent Simulant. *Chem. Commun.* **2015**, *51*, 10925–10928.

(55) Liu, Y.; Moon, S.-Y.; Hupp, J. T.; Farha, O. K. Dual-Function Metal-Organic Framework as a Versatile Catalyst for Detoxifying Chemical Warfare Agent Simulants. *ACS Nano* **2015**, *9*, 12358–12364.

(56) Peterson, G. W.; Moon, S.-Y.; Wagner, G. W.; Hall, M. G.; DeCoste, J. B.; Hupp, J. T.; Farha, O. K. Tailoring the Pore Size and Functionality of UiO-Type Metal-Organic Frameworks for Optimal Nerve Agent Destruction. *Inorg. Chem.* **2015**, *54*, 9684–9686.

(57) Moon, S. Y.; Prousaloglou, E.; Peterson, G. W.; DeCoste, J. B.; Hall, M. G.; Howarth, A. J.; Hupp, J. T.; Farha, O. K. Detoxification of Chemical Warfare Agents Using a Zr₆-Based Metal-Organic Framework/Polymer Mixture. *Chem.—Eur. J.* **2016**, *22*, 14864–14868.

(58) Moon, S.-Y.; Howarth, A. J.; Wang, T.; Vermeulen, N. A.; Hupp, J. T.; Farha, O. K. A Visually Detectable PH Responsive Zirconium Metal-Organic Framework. *Chem. Commun.* **2016**, *52*, 3438–3441.

(59) Troya, D. Reaction Mechanism of Nerve-Agent Decomposition with Zr-Based Metal Organic Frameworks. *J. Phys. Chem. C* **2016**, *120*, 29312–29323.

(60) Wang, G.; Sharp, C.; Plonka, A. M.; Wang, Q.; Frenkel, A. I.; Guo, W.; Hill, C.; Smith, C.; Kollar, J.; Troya, D.; et al. Mechanism and Kinetics for Reaction of the Chemical Warfare Agent Simulant, DMMP(g), with Zirconium(IV) MOFs: An Ultrahigh-Vacuum and DFT Study. *J. Phys. Chem. C* **2017**, *121*, 11261–11272.

(61) Islamoglu, T.; Atilgan, A.; Moon, S.-Y.; Peterson, G. W.; DeCoste, J. B.; Hall, M.; Hupp, J. T.; Farha, O. K. Cerium(IV) vs Zirconium(IV) Based Metal-Organic Frameworks for Detoxification of a Nerve Agent. *Chem. Mater.* **2017**, *29*, 2672–2675.

(62) Chen, H.; Liao, P.; Mendonca, M. L.; Snurr, R. Q. Insights into Catalytic Hydrolysis of Organophosphate Warfare Agents by Metal-

Organic Framework NU-1000. *J. Phys. Chem. C* **2018**, *122*, 12362–12368.

(63) Momeni, M. R.; Cramer, C. J. Dual Role of Water in Heterogeneous Catalytic Hydrolysis of Sarin by Zirconium-Based Metal-Organic Frameworks. *ACS Appl. Mater. Interfaces* **2018**, *10*, 18435–18439.

(64) Ryu, S. G.; Kim, M.-K.; Park, M.; Jang, S. O.; Kim, S. H.; Jung, H. Availability of Zr-Based MOFs for the Degradation of Nerve Agents in All Humidity Conditions. *Microporous Mesoporous Mater.* **2019**, *274*, 9–16.

(65) Wepasnick, K. A.; Li, X.; Mangler, T.; Noessner, S.; Wolke, C.; Grossmann, M.; Gantefoer, G.; Fairbrother, D. H.; Bowen, K. H. Surface Morphologies of Size-Selected $\text{Mo}_{100\pm 2.5}$ and $(\text{MoO}_3)_{67\pm 1.5}$ Clusters Soft-Landed onto HOPG. *J. Phys. Chem. C* **2011**, *115*, 12299–12307.

(66) Whittle, E.; Dows, D. A.; Pimentel, G. C. Matrix Isolation Method for the Experimental Study of Unstable Species. *J. Chem. Phys.* **1954**, *22*, 1943.

(67) Moulder, J. F.; Stickle, W. F.; Sobol, P. E.; Bomben, K. D. Appendix F. Atomic Sensitivity Factors for X-Ray Sources at 54.7°. *Handbook of X-ray Photoelectron Spectroscopy*; Physical Electronics Division, Perkin-Elmer Corporation, 1992; p 253.

(68) Sun, Y.-M.; Lozano, J.; Ho, H.; Park, H. J.; Veldman, S.; White, J. M. Interfacial Silicon Oxide Formation during Synthesis of ZrO_2 on Si(100). *Appl. Surf. Sci.* **2000**, *161*, 115–122.

(69) Zhang, N. L.; Song, Z. T.; Wan, Q.; Shen, Q. W.; Lin, C. L. Interfacial and Microstructural Properties of Zirconium Oxide Thin Films Prepared Directly on Silicon. *Appl. Surf. Sci.* **2002**, *202*, 126–130.

(70) Kim, M.-S.; Ko, Y.-D.; Hong, J.-H.; Jeong, M.-C.; Myoung, J.-M.; Yun, I. Characteristics and Processing Effects of ZrO_2 Thin Films Grown by Metal-Organic Molecular Beam Epitaxy. *Appl. Surf. Sci.* **2004**, *227*, 387–398.

(71) Brenier, R.; Mugnier, J.; Mirica, E. XPS Study of Amorphous Zirconium Oxide Films Prepared by Sol-Gel. *Appl. Surf. Sci.* **1999**, *143*, 85–91.

(72) Zhang, Z.; Zandkarimi, B.; Alexandrova, A. N. Ensembles of Metastable States Govern Heterogeneous Catalysis on Dynamic Interfaces. *Acc. Chem. Res.* **2020**, *53*, 447–458.

(73) Zandkarimi, B.; Alexandrova, A. N. Dynamics of Subnanometer Pt Clusters Can Break the Scaling Relationships in Catalysis. *J. Phys. Chem. Lett.* **2019**, *10*, 460–467.

(74) Zhai, H.; Alexandrova, A. N. Local Fluxionality of Surface-Deposited Cluster Catalysts: The Case of Pt_7 on Al_2O_3 . *J. Phys. Chem. Lett.* **2018**, *9*, 1696–1702.

(75) Baxter, E. T.; Ha, M.-A.; Cass, A. C.; Alexandrova, A. N.; Anderson, S. L. Ethylene Dehydrogenation on $\text{Pt}_{4,7,8}$ Clusters on Al_2O_3 : Strong Cluster Size Dependence Linked to Preferred Catalyst Morphologies. *ACS Catal.* **2017**, *7*, 3322–3335.

(76) Busolt, U.; Cottancin, E.; Socaciu, L.; Röhr, H.; Leisner, T.; Wöste, L. Diffusion and aggregation of Ag_n -clusters ($n = 2-9$) on HOPG probed by fs-two-photon-photoemission. *Eur. Phys. J. D* **2001**, *16*, 297–300.

(77) Howells, A.; Hung, L.; Chottiner, G. S.; Scherson, D. A. Effects of Substrate Defect Density and Annealing Temperature on the Nature of Pt Clusters Vapor Deposited on the Basal Plane of Highly Oriented Pyrolytic Graphite. *Solid State Ionics* **2002**, *150*, 53–62.

(78) Kushvaha, S. S.; Yan, Z.; Xiao, W.; Wang, X.-S. Surface Morphology of Crystalline Antimony Islands on Graphite at Room Temperature. *J. Phys.: Condens. Matter* **2006**, *18*, 3425–3434.

(79) Al-Hada, M.; Peters, S.; Peredkov, S.; Neeb, M.; Eberhardt, W. Nanoisland Formation of Small Ag_n -clusters on HOPG as Determined by Inner-shell Photoionisation Spectroscopy. *Surf. Sci.* **2015**, *639*, 43–47.

(80) Holme, T.; Zhou, Y.; Pasquarelli, R.; O'Hayre, R. First Principles Study of Doped Carbon Supports for Enhanced Platinum Catalysts. *Phys. Chem. Chem. Phys.* **2010**, *12*, 9461–9468.

(81) Tang, X.; Bowen, K. H.; Calvo, F. Self-assembly of $(\text{WO}_3)_3$ Clusters on a Highly Oriented Pyrolytic Graphite Surface and

Nanowire Formation: A Combined Experimental and Theoretical Study. *Phys. Chem. Chem. Phys.* **2017**, *19*, 31168–31176.

(82) Colón-Ortiz, J.; Landers, J. M.; Gordon, W. O.; Balboa, A.; Karwacki, C. J.; Neimark, A. V. Disordered Mesoporous Zirconium (Hydr)Oxides for Decomposition of Dimethyl Chlorophosphate. *ACS Appl. Mater. Interfaces* **2019**, *11*, 17931–17939.

(83) Bluhm, H. Photoelectron Spectroscopy of Surfaces under Humid Conditions. *J. Electron Spectrosc. Relat. Phenom.* **2010**, *177*, 71–84.

(84) He, M.; Ekerdt, J. G. Methanol Formation on Zirconium Dioxide. *J. Catal.* **1984**, *90*, 17–23.

(85) Badlani, M.; Wachs, I. E. Methanol: A “Smart” Chemical Probe Molecule. *Catal. Lett.* **2001**, *75*, 137–149.

(86) Tatibouët, J. M. Methanol Oxidation as a Catalytic Surface Probe. *Appl. Catal., A* **1997**, *148*, 213–252.

(87) Yaripour, F.; Baghaei, F.; Schmidt, I.; Perregaard, J. Catalytic Dehydration of Methanol to Dimethyl Ether (DME) Over Solid-Acid Catalysts. *Catal. Commun.* **2005**, *6*, 147–152.

(88) Alharbi, W.; Kozhevnikova, E. F.; Kozhevnikov, I. V. Dehydration of Methanol to Dimethyl Ether over Heteropoly Acid Catalysts: The Relationship between Reaction Rate and Catalyst Acid Strength. *ACS Catal.* **2015**, *5*, 7186–7193.

(89) Carr, R. T.; Neurock, M.; Iglesia, E. Catalytic Consequences of Acid Strength in the Conversion of Methanol to Dimethyl Ether. *J. Catal.* **2011**, *278*, 78–93.

(90) Bianchi, D.; Chafik, T.; Khalfallah, M.; Teichner, S. Intermediate Species on Zirconia Supported Methanol Aerogel Catalysts V. Adsorption of Methanol. *Appl. Catal., A* **1995**, *123*, 89–110.

(91) Walenta, C. A.; Xu, F.; Tesvara, C.; O'Connor, C. R.; Sautet, P.; Friend, C. M. Facile Decomposition of Organophosphonates by Dual Lewis Sites on a $\text{Fe}_3\text{O}_4(111)$ Film. *J. Phys. Chem. C* **2020**, *124*, 12432–12441.

(92) Dilara, P. A.; Vohs, J. M. Structure Sensitivity in the Reaction of Methanol on ZrO_2 . *Surf. Sci.* **1994**, *321*, 8–18.

(93) Schweigert, I. V.; Gunlycke, D. Hydrolysis of Dimethyl Methylphosphonate by the Cyclic Tetramer of Zirconium Hydroxide. *J. Phys. Chem. A* **2017**, *121*, 7690–7696.

(94) Plonka, A. M.; Wang, Q.; Gordon, W. O.; Balboa, A.; Troya, D.; Guo, W.; Sharp, C. H.; Senanayake, S. D.; Morris, J. R.; Hill, C. L.; et al. In Situ Probes of Capture and Decomposition of Chemical Warfare Agent Simulants by Zr-Based Metal Organic Frameworks. *J. Am. Chem. Soc.* **2017**, *139*, 599–602.

(95) Long, J. W.; Chervin, C. N.; Balow, R. B.; Jeon, S.; Miller, J. B.; Helms, M. E.; Owrutsky, J. C.; Rolison, D. R.; Fears, K. P. Zirconia-Based Aerogels for Sorption and Degradation of Dimethyl Methylphosphonate. *Ind. Eng. Chem. Res.* **2020**, *59*, 19584–19592.